# Distribution of Hydrophobic Ions and Their Counterions at an Aqueous Liquid−Liquid Interface: A Molecular Dynamics Investigation

**Benoît Schnell, Rachel Schurhammer, and Georges Wipff***

*Laboratoire MSM, Institut de Chimie, Université Louis Pasteur, UMR CNRS 7551, 4, rue B. Pascal, 67 000 Strasbourg, France*

*Received: September 29, 2003; In Final Form: December 9, 2003*

We report a molecular dynamics study on the distribution of spherical hydrophobic ions $S^+$ and $S^-$ (radius $\approx 5.5$ Å) and hydrophilic counterions (halide $X^-$; alkali $M^+$) at a water−"oil" interface, where "oil" is modeled by chloroform. The results reveal the surface activity of $S^+$ and $S^-$, with marked counterion effects. The $S^+S^-$ salt fully adsorbs at the interface, which is electrically neutral, while in the $S^+X^-$ series, the anion concentration near the interface decreases in the Hofmeister order $I^- > Br^- > Cl^- > F^-$, thus increasing the change in interfacial electrostatic potential $\Delta\phi$. A similar effect is observed with the $S^-M^+$ salts, when $Cs^+$ is compared to $Na^+$. We also investigate the effect of ion charge sign reversal, and find a larger $\Delta\phi$ for $S^+ Na^-$ than $S^- Na^+$ salts, in relation with the higher hydration of the fictitious $Na^-$ anion compared to the isosteric $Na^+$ cation. The effect of the magnitude of the ion charge is studied with the divalent $S^{2+}$ vs $S^{2-}$ ions and $Na^-$ vs $Na^+$ counterions. Despite their mutual repulsion, the $S^{2+}$ or $S^{2-}$ like-charged species tend to self-aggregate at the interface and in water as a result of hydrophobic association and, again, differences in distributions are observed upon sign reversal. With regard to the treatment of electrostatics, the Ewald and Reaction Field methods qualitatively yield similar trends, but the latter underestimates the repulsion between like ions at the interface and thus exaggerates the calculated difference in interfacial potential $\Delta\phi$. When compared to standard calculations, our results point to the importance of the treatment of cutoff boundaries on the distribution of hydrophilic counterions near the interface. Implications of these results concerning the mechanism of assisted ion transfer are discussed.

## Introduction

A precise knowledge of ion distribution at the interface between two immiscible electrolyte solutions (ITIES) is of interest in many areas of physical chemistry such as electrochemistry, phase transfer catalysis, drug availability, ion separation by liquid−liquid extraction, and liquid chromatography, as well as membranes mimics.[1−5] It also has implications in environmental processes or atmospheric pollution. Little is known, however, about the microscopic structure of the interface, and most of our knowledge relies on thermodynamics,[6] electrochemical measurements of current, potentials, and surface tension, which give information on the concentration ("activity") of the ions at the interface[7] and on their transfer across the interface.[2,8] Structural features may be investigated by surface spectroscopy[9,10] and X-ray or neutron reflectivity,[11,12] but precise information at ITIES is rather limited. An important source of information—or, at least, stimulating microscopic pictures—comes from molecular dynamics (MD) or Monte Carlo simulation techniques, which explicitly account for the granularity of the systems and of statistical features of solvation. Pioneering simulations on ions at aqueous interfaces have been reported by Valleau and Torrie,[13] Jorgensen,[14] Heinzinger,[15,16] and Benjamin.[17] Accounts can be found in refs 18−20. Layers or micelles of cationic [21] or anionic [22] surfactants have also been extensively studied.

We have been interested in liquid−liquid interfaces in the context of assisted liquid−liquid extraction of ions and found that most of the hydrophobic partners involved in that process (uncomplexed and complexed extractants, counterions) are surface active[23−27] and adsorb at the water−"oil" interface, instead of spontaneously diffusing to the oil phase. This contrasts with hydrophilic ions (e.g. $Cl^-$, $NO_3^-$ anions, or metallic cations) which were found to be "repelled" by the interface. Of particular interest was the finding that hydrophobic ions lacking the classical amphiphilic topology (polar head flanked by a hydrophobic chain) can also be surface active. This was the case for the flat picrate anions or guanidinium cations, for tetrahedral ions such as $AsPh_4^+$ and $BPh_4^-$ [28,29] or the "peanut-shaped" chlorinated cobalt dicarbollides.[30,31] Even large spherical model ions $S^+$ or $S^-$, used as "perfect models" in the context of the TATB (tetraphenylarsonium tetraphenylborate) hypothesis,[32] were found to concentrate and form a monolayer at the interface.[33−36] More surprising was the relationship with their neutralizing $Cl^-$ or $Na^+$ counterions which concentrated in the bulk water phase, separated from the interfacial ionic layer by a slice of water. This picture contrasted with the classical model of double layer at electrified interfaces, in which the concentration of counterions smoothly decreases as their distance to the interface increases (Gouy−Chapman-type models).[37,38] We note that these simulations used standard treatments of nonbonded interactions and relatively small (12−15 Å) residue-based cutoffs for the Coulombic interactions.

We thus decided to reinvestigate the question of ion distribution at the water−chloroform interface using corrected treatments of "long-range" electrostatic forces, i.e., compare the Ewald summation and the reaction field "RF" methods. Our

* Address correspondence to this author. E-mail: wipff@chimie.u-strasbg.fr.

10.1021/jp036896m CCC: $27.50 
Published on Web 01/23/2004

**TABLE 1: Lennard-Jones Parameters of the Simulated Ions**

| | $F^-$ | $Cl^-$ | $Br^-$ | $I^-$ | $Na^\pm$ | $Cs^+$ | $S^\pm$ |
|---|---|---|---|---|---|---|---|
| **R*** (Å) | 1.850 | 2.495 | 2.679 | 3.005 | 1.868 | 3.395 | 5.500 |
| $\epsilon$ (kcal/mol) | 0.2000 | 0.1070 | 0.0858 | 0.0522 | 0.0028 | 0.0001 | 0.1000 |

**TABLE 2: Characteristics of the Simulated Systems: Number of Solvent Molecules, Box Size, and Simulated Time**

| system | $N_{clf} + N_{wat}$ | $V_x \times V_y \times (V_{z-clf} + V_{z-wat})$ (Å$^3$) | time (ns) |
|---|---|---|---|
| $S^+ S^-$ | 454 + 2041 | 37.8 × 36.9 × (43.8 + 43.8) | 0.6 |
| $S^+ Cl^-$ | 454 + 2041 | 37.8 × 36.9 × (43.8 + 43.8) | 0.6 |
| $S^- Na^+$ | 454 + 2041 | 37.8 × 36.9 × (43.8 + 43.8) | 0.6 |
| 16 $S^+ S^-$ | 765 + 2674 | 39.0 × 39.0 × (54.2 + 44.2) | 1.5 |
| 16 $S^+ S^-$ [a] | 765 + 2674 | 40.0 × 40.0 × (51.2 + 51.2) | 1.5 |
| 16$S^+ F^-$ | 765 + 2674 | 47.7 × 47.7 × (45.7 + 35.5) | 1.5 |
| 16$S^+ Cl^-$ | 765 + 2674 | 47.7 × 47.7 × (45.7 + 35.5) | 1.5 |
| 16 $S^+ Br^-$ | 765 + 2674 | 47.7 × 47.7 × (45.7 + 35.5) | 1.5 |
| 16 $S^+ I^-$ | 765 + 2674 | 47.7 × 47.7 × (45.7 + 35.5) | 1.5 |
| 16 $S^- Na^+$ | 765 + 2674 | 47.7 × 47.7 × (45.7 + 35.5) | 1 |
| 16 $S^+ Na^-$ | 765 + 2674 | 47.7 × 47.7 × (45.7 + 35.5) | 1 |
| 8 $S^{2-}$; 16 $Na^+$ | 799 + 2538 | 47.7 × 47.7 × (47.7 + 33.7) | 1 |
| 8 $S^{2+}$; 16 $Na^-$ | 799 + 2538 | 47.7 × 47.7 × (47.7 + 33.7) | 1 |

[a] The ion layer is initially perpendicular, instead of parallel to the interface.

main aims are to investigate (i) the surface activity of $S^+$ and $S^-$ hydrophobic ions and (ii) their relationship with neutralizing counterions of different sizes (in relation with the Hofmeister effect,[39] we compare the different halides $X^-$ as counterions of $S^+$, and $Na^+$ vs $Cs^+$ counterions of $S^-$), (iii) the effect of the magnitude of the charge on hydrophobic ions, thus modeling divalent $S^{2+}$ and $S^{2-}$ species, and (iv) the effect of ion charge inversion (with fixed ion "size", i.e., fixed van der Waals parameters) on the interfacial distribution, by comparing $S^-$/ $S^+$ and $S^{2-}$/ $S^{2+}$ with $Na^+$/$Na^-$ as counterions. Note that the anionic counterpart of $Na^+$, hereafter noted $Na^-$ for convenience, is purely fictitious. The simulated systems contain up to 16 positive and 16 negative charges in the simulation box, corresponding to aqueous concentrations of about 0.15 mol/L. Several methodological tests are also presented.

## Methods

The simulations were performed with AMBER5.0[40] where the potential energy $U$ is described by a sum of bond and angle deformation energies, and pairwise additive 1-6-12 (electrostatic + van der Waals) interactions between nonbonded atoms.

$$U = \sum_{bonds} K_r (r - r_{eq})^2 + \sum_{angles} K_\theta (\theta - \theta_{eq})^2 + \sum_{i<j} [q_i q_j / R_{ij} - 2\epsilon_{ij}(R_{ij}^*/R_{ij})^6 + \epsilon_{ij}(R_{ij}^*/R_{ij})^{12}]$$

The R* and $\epsilon$ ion parameters are given in Table 1. The S ions ($S^-$, $S^+$, $S^{2-}$, and $S^{2+}$) are isosteric and similar in size to $AsPh_4^+$ or $BPh_4^-$. The $Na^+$ and $Cs^+$ parameters are adapted from Åqvist[41] and those of $F^-$, $Cl^-$, $Br^-$, and $I^-$ are from Berny et al.[42] The fictitious $Na^-$ ion has the same R* and $\epsilon$ parameters as $Na^+$. As solvent models, we used TIP3P for water [43] and OPLS for chloroform,[44] fitted on the pure liquid properties. Tests were also performed with the polarizable water model of Chang and Dang[45] and with a polarization term on the anions (with atomic polarizabilities $\alpha_F = 0.32$ Å$^3$ and $\alpha_I = 4.69$ Å$^3$ from Applequist et al.[46]). The simulated solvent systems and simulation conditions are summarized in Table 2. All O−H, H···H, C−Cl, and Cl···Cl solvent "bonds" were constrained with SHAKE,[40] using a time step of 2 fs. The temperature was monitored by coupling the system to a thermal bath at the reference temperature of 300 K with a relaxation time of 0.4 ps.

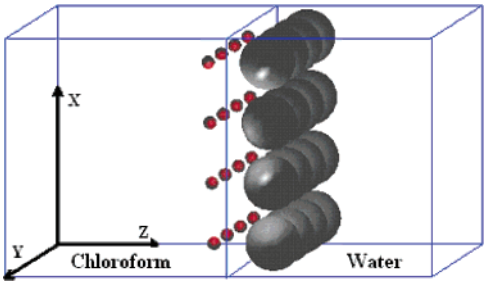


**Figure 1.** The chloroform−water interface with the initial arrangement of 16 $S^-$ $Na^+$ ions.

The evaluation of the potential energy in electrolytes is a difficult task due to the electrostatic component.[47,48] We used the Ewald summation method[49] (particle mesh Ewald "PME" approximation[40,50]) for all systems, thus including in principle long-range interactions. We also tested the reaction field (RF)[51] method, which assumes that the system contained within the cutoff distance is immersed in a polarizable dielectric medium with which it interacts. Discussions can be found in refs 52 and 53, while alternative approaches (e.g. 2D-Ewald summation) are presented in refs 16 and 54.

The water/chloroform interface has been built as indicated in refs 55 and 56, starting with adjacent boxes of pure water and chloroform (Figure 1). The solutes were initially placed at the interface, equally shared between the two solvent phases, with "reversed" arrangements, i.e., with the hydrophilic ions on the organic side and the hydrophobic ones on the aqueous side of the interface. This is to avoid being initially trapped in an energy minimum. The systems were first energy minimized by 100 steps of steepest descent followed by 900 steps of conjugated gradient methods. Then MD was run for 50 ps in the ($N$,$V$,$T$) ensemble for 50 ps with frozen ions (BELLY option of AMBER), followed by 25 ps of free dynamics plus 75 ps of dynamics in the ($N$,$P$,$T$) ensemble. The temperature was maintained at 300 K via a weak coupling to a thermostat[57] with a relaxation time of 0.4 ps. The production stage was 0.6 ns long for the diluted salts and 1.5 ns long for the concentrated salts and was performed at constant volume. Tests at a constant pressure of 1 atm were also performed. The systems were represented with 3D periodic boundary conditions, thus with alternating slabs of water and chloroform.

The protocol of the mixing−demixing simulations was similar to the one described in ref 56 and proceeded in three steps. (i) First, 100 ps equilibration simulation at 300 K with the solute placed at the preformed water-chloroform interface to ensure that solvent densities in the bulk regions are correct, (ii) simulation at 500 K at constant volume with biased potentials (electrostatics divided by a factor 100) to mix the solvents, and (iii) after energy minimization, the demixing MD simulation started by resetting the temperature at 300 K and all charges at their reference values.

The results have been analyzed as described in ref 55. The position of the interface was dynamically defined as the intersection between the water and oil smoothed density. The percentage of species "near the interface" was calculated from the statistical average of these species that are within a distance of 8 Å from the interface. According to solvent density curves, this distance corresponds to about half of the interfacial width. We define the density of solvents and solutes (g·cm$^{-3}$) at a $z$-position by their mass per volume unit ($d\nu = xy\ dz$), taking

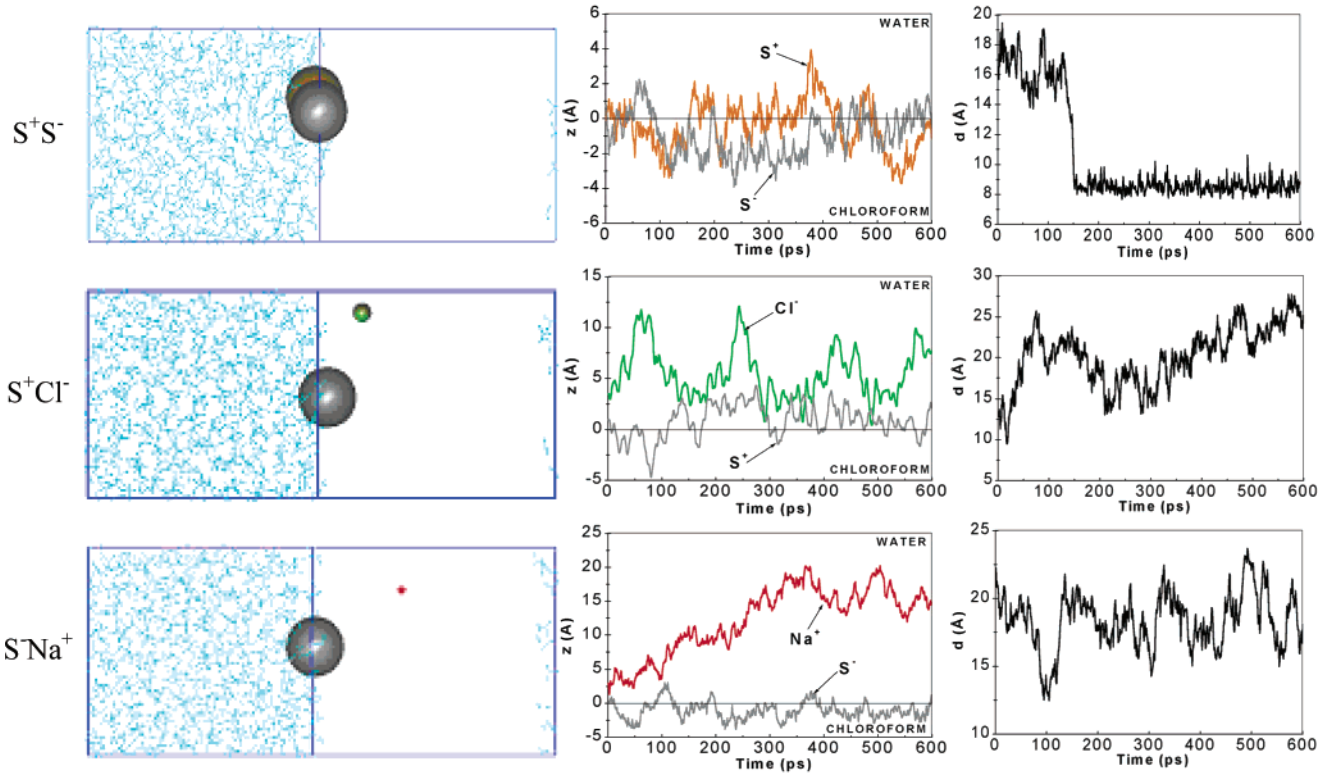


**Figure 2.** Diluted solutions of $S^+ S^-$, $S^+ Cl^-$, and $S^- Na^+$ salts at the interface. From left to right: snapshots at 0.6 ns, distances between the ions and the interface and interionic distances as a function of time. PME calculations.

an arbitrary mass of 75 g·mol$^{-1}$ for the S spheres. The average electrostatic potential $\phi(z)$ was calculated in $xy$ slices of 0.5 Å thickness, as an average over 5 × 5 grids of about 25 Å$^2$ each, including the contributions of all ions and solvent atoms of the simulated box or of its nearest periodic image. A discussion can be found in ref 58. Insights into energy components were obtained from the average interactions between selected groups (cations, anions, water, chloroform), calculated with a 15 Å cutoff + RF correction. Averages were performed during the last 0.3 ns. The average distribution of ions and solvent around a given species is characterized by the corresponding radial distribution function ("RDF"), averaged over all equivalent species.

## Results

Unless otherwise specified, the results reported in this section were obtained with the PME Ewald summation technique. We will compare them with the RF results in the discussion section. The first important feature, common to all simulated systems, is the adsorption of the hydrophobic $S^+$ or $S^-$ ions at the water−chloroform interface, and the migration of the hydrophilic counterions from the organic to the aqueous phase. In a few cases, some $S^+$ ions migrated to the aqueous phase. No transfer of $S^+$ or $S^-$ to the organic phase was observed, which contrasts to what was reported for the analogous $AsPh_4^+ Cl^-$ or $BPh_4^- Na^+$ systems.[34] We note that the latter were simulated with a standard treatment of the electrostatics at the boundaries, causing different relationships with the counterions (vide infra).

The observed detailed distributions depend on the ion concentration, on the nature of counterions, and on the sign and magnitude of the ionic charges. We first describe the diluted systems with one ion pair ($S^+ S^-$, $S^+ Cl^-$, and $S^- Na^+$) in the box only, as a reference for the more concentrated ones. We next examine the effect of $X^-$ halide counterions in $S^+ X^-$ salts and of $Na^+$ vs $Cs^+$ counterions in $S^- M^+$ salts. This is followed by the question of ion charge (sign and magnitude).

The analysis mainly focuses on the ion distributions, illustrated by typical snapshots of the last configurations and by the average density curves. The solvent density profiles are similar to those obtained for the corresponding neat interface.[24] On the average, the interface is narrow and sharp, about 10−15 Å in width, which corresponds to the size of a few fluctuating solvent molecules. Beyond this region, with a few exceptions, no solvent mixing is observed. Instantaneously, however, the water and oil surfaces are not flat, but display protuberances of up to ≈7 Å corresponding to the granularity of the solvent molecules and of the adsorbed ions.

**1. Surface Activity of Hydrophobic $S^+$ or $S^-$ Ions in Diluted Solutions of $S^+ Cl^-$, $S^+ S^-$, and $S^+ Na^-$ Salts.** The simulations of diluted solutions of $S^+ Cl^-$, $S^+ S^-$, and $S^+ Na^-$ salts (concentrations are ≈ 0.01 mol/L) started with the two ions at the interface ($z = 0$), 16 Å apart. During the dynamics, $S^+$ and $S^-$ oscillated at the interface, while the $Cl^-$ or $Na^+$ counterions diffused to water (see Figure 2). Depending on the system, one also notices different ion−counterion relationships. The $S^+ S^-$ salt formed in less than 0.3 ns an intimate ion pair at the interface ($dS\cdots S \approx 8$ Å), while the $S^+ Na^-$ and $S^+ Cl^-$ salts fully dissociated ($d > 20$ Å). According to an energy component analysis (see Table 3), $S^+$ and $S^-$ interact more with water (from −17 to −43 ± 6 kcal/mol) than with chloroform (≈−10 kcal/mol), thus preventing their migration to the chloroform phase. They do not migrate to water, however, because of unfavorable cavitation energies.[59,60] At the interface, $S^-$ and $S^+$ are more hydrated when the counterions are dissociated (−43 vs −35 ± 6 kcal/mol, with $Na^+$ or $Cl^-$ counterions, respectively) than when they are paired and thus less accessible to water (−31 vs −17 ± 6 kcal/mol, respectively, in the $S^- S^+$ salt). For the same reason, $S^-$ and $S^+$ are less hydrated than in bulk water (−64 vs −41 kcal/mol, respectively,

**TABLE 3: Diluted Solutions of $S^+S^-$, $S^+Cl^-$, $S^-Na^+$ Ions at the Interface: Average Interaction Energies (kcal·mol$^{-1}$) between the Anion, the Cation, and the Solvents**

| | $S^+Cl^-$ | $Na^+S^-$ | $S^+S^-$ |
|---|---|---|---|
| $d$(S···interface)[a] | $0.8 \pm 1.0$ | $-0.8 \pm 1.1$ | $-0.8 \pm 1.5$[b] |
| $E_{anion/wat}$ | $-96 \pm 14$ | $-43 \pm 6$ | $-31 \pm 6$ |
| $E_{cation/wat}$ | $-35 \pm 5$ | $-160 \pm 9$ | $-17 \pm 7$ |
| $E_{anion/clf}$ | $0 \pm 1$ | $-9 \pm 4$ | $-8 \pm 3$ |
| $E_{cation/clf}$ | $-10 \pm 3$ | $0 \pm 1$ | $-12 \pm 4$ |

[a] Distance (in Å) from the density peak of the ion and the starting interface. [b] Value for $d(S^+\cdots\text{interface})$. The $d(S^-\cdots\text{interface})$ distance is $-0.4 \pm 0.9$ Å.

calculated in the same conditions; see also refs 35 and 61). Comparing now the $S^-$ vs $S^+$ hydration at the interface, one sees that the anion is more attracted by water than the cation is, following the same trend as in pure water.

Species that adsorb at the interface are by definition surface active and should accumulate at the interface. Like-charged ions, however, repell each other, which opposes their concentration, an effect that may be diminished by the presence of neutralizing counterions. The final ion distribution is thus described in the next section.

**2. Concentrated Solutions of $S^+X^-$ and $S^-M^+$ Monovalent Ions at the Interface ($X^- = F^-$ to $I^-$; $M^+ = Na^+$, $Cs^+$).** In this section, we consider electrolyte solutions containing $2 \times 16$ ions in the simulation box. Seven electrolytes have been considered, allowing us to compare the effect of counterions size and hydrophilicity in the $S^+X^-$ (X = F / Cl / Br / I / S) and $S^-M^+$ series (M = Na vs Cs).

In the case of the $S^+S^-$ salt, all ions form at the end of the dynamics a $4 \times 4$ grid at the interface that is therefore electrically neutral. Since this closely resembles the starting configuration, we decided to simulate again that system, starting with another configuration, i.e., a $4 \times 4$ grid perpendicular to the interface and shared between the two solvent phases. After 1.5 ns of dynamics, the ion distribution was quasiidentical with these two arrangements.

In the $S^+X^-$ solutions with halides, marked counterion effects are observed (see Figure 3 and Table 4). The percentage of $S^+$ species at the interface increases with the size of $X^-$. The $X^-$ anions generally dilute in the aqueous phase but, as they get bigger, a clear peak of concentration develops near the interface (Figure 3) where their proportion increases from 38% ($F^-$) to 42% ($Cl^-$), 46% ($Br^-$), and 52% ($I^-$). Thus, it happens as if the less hydrophilic anions are more attracted by the interfacial $S^+$ species, an effect that is consistent with the evolution of average $S^+\cdots X^-$ attraction energies which regularly increase from $F^-$ ($-14$ kcal/mol) to $I^-$ ($-31$ kcal/mol; see Table 4). The most hydrophobic anions tend to form intimate ion pairs with $S^+$, as seen by the average cation−anion RDFs (Figure 4) which peak at $\approx$7 Å for $I^-$ and $Br^-$. The peak is most pronounced for the biggest anion, and integrates (up to 9 Å) to 0.96 $I^-$ counterions on the average, per $S^+$. Within the same radius one finds 0.45 $Br^-$, 0.35 $Cl^-$, and 0.22 $F^-$ ions only, showing that $S^+X^-$ ion pairing decreases with the decreasing anion size and increasing hydrophilicity.[62]

Similar counterion effects are observed in the distribution of $S^-M^+$ salts, with $Na^+$ vs $Cs^+$ cations. In both cases, the $S^-$ ions form a negatively charged interfacial layer, which is more uniform with $Cs^+$ than with $Na^+$. Near the interface, one finds 50% of $Na^+$ and 80% of $Cs^+$ cations, together with 93% and 100% of $S^-$ species, respectively. Thus cation−anion attractions are larger with $Cs^+$ than with $Na^+$ counterions ($-62$ vs $-26$ kcal/mol), due to enhanced ion pairing, as shown by the RDFs which markedly peak in the case of $Cs^+$ (Figure 4). Integration yields 1.60 $Cs^+$ and 0.76 $Na^+$ cations, on the average, coordinated to a given $S^-$. Thus, $S^-M^+$ ion pairing at the interface again increases with the size of the $M^+$ counterion and, as a result, $S^-$ is more shielded and interacts less with water with $Cs^+$ than with $Na^+$ as counterion ($-15$ vs $-52 \pm 3$ kcal/mol).

The asymmetry of charge distribution near the interface leads to electrical properties, that we characterized by the evolution of the electrostatic potential $\phi(z)$ and its variation $\Delta\phi$ upon the interface crossing, where $\Delta\phi$ was calculated as the difference between the $\phi_{Max}$ and $\phi_{Min}$ values for a given solute. The plot of $\phi(z)$ (see Figure 5) nicely reflects the ion distribution near the interface. In the $S^+X^-$ series, $\phi(z)$ displays a similar profile with the four halide counterions:[63] it is positive on the chloroform side ($z < 0$), negative on the water side of the interface ($z > 5$ Å), and displays a small maximum at $z \approx -2$ Å. On the water side, interesting evolutions are noted, as $\phi(z)$ becomes less negative with the bigger counterions, and the difference $\Delta\phi$ nicely follows the order (in V) $F^-$ (1.49) > $Cl^-$ (1.46) > $Br^-$ (1.32) > $I^-$ (1.15) $\gg$ $S^-$ (0.30).[64] In the case of the $S^-M^+$ electrolytes (see Figure 5), $\phi(z)$ is close to zero near the center of the solvent slabs and negative near the interface, due to the dominant contribution of the $S^-$ ions. The interface is, however, more neutralized by the $Cs^+$ than by the $Na^+$ counterions, leading to a smaller $\Delta\phi$ with $Cs^+$ (0.33 V) than with $Na^+$ (0.56 V).

**3. The Effect of Ions Sign and Charge: $S^+$, $S^-$, $S^{2-}$, $S^{2+}$, and Their Counterions at the Interface.** As noted in the first section and in refs 33, 35, 36, and 61, inversion of the sign of the $S^+/S^-$ ion charge changes the solvation properties and, likely, the ion distribution at the interface. Here, we investigate the role of sign reversal of the $S^\pm$ charge and of their counterions, as well as the effect of the magnitude of the charge (from $S^\pm$ to $S^{2\pm}$), keeping the solution electroneutral. The studied systems have 16 positive and 16 negative charges: 16 $S^-Na^+$, 16 $S^+Na^-$, 8 ($S^{2+}$, $2Na^-$) and 8 ($S^{2-}$, $2Na^+$). The final ion distributions and density curves are shown in Figure 6 and the main results are summarized in Table S1.

We first discuss the $S^-Na^+$ vs $S^+Na^-$ solutions, in which the S monovalent ions concentrate at the interface and their counterions sit in water, with interesting differences, though. The proportion of $S^-$ ions at the surface (93%) is larger than the $S^+$ proportion ($70 \pm 2$%). It thus looks as if the $S^-$ species are less attracted by water than the $S^+$ are. This interpretation is, however, not supported by the energy component analysis at the interface (see $S^+Cl^-$ and $S^-Na^+$ monomers; section 1) or in bulk water, according to which $S^-$ is better hydrated than $S^+$. We believe that $Na^+$ vs $Na^-$ counterions play an important role. Indeed, the latter are much more hydrophilic than the former, following the same trends as the $S^+$ or $S^-$ ions. Their interaction energies with water are $-154$ and $-266 \pm 5$ kcal/mol, respectively, on the average, which is close to the energies obtained in a pure water solution ($-158$ and $-271 \pm 9$ kcal/mol, respectively). As seen in Figure 6, the $Na^-$ ions are more deeply immersed in water and display less ion pairing with $S^+$ than their $Na^+S^-$ analogues do, and thus neutralize less the $S^+$ layer. This is supported by the S···Na RDFs (Figure S1), which integrate (up to 9.5 Å) to 0.76 $Na^+$ cation per $S^-$, and only to 0.30 $Na^-$ anion per $S^+$, on the average. One thus finds more $Na^+$ (50%) than $Na^-$ ($25 \pm 8$%) counterions near the interface. Thus, two main effects contribute to drag $S^+$ ions to water:

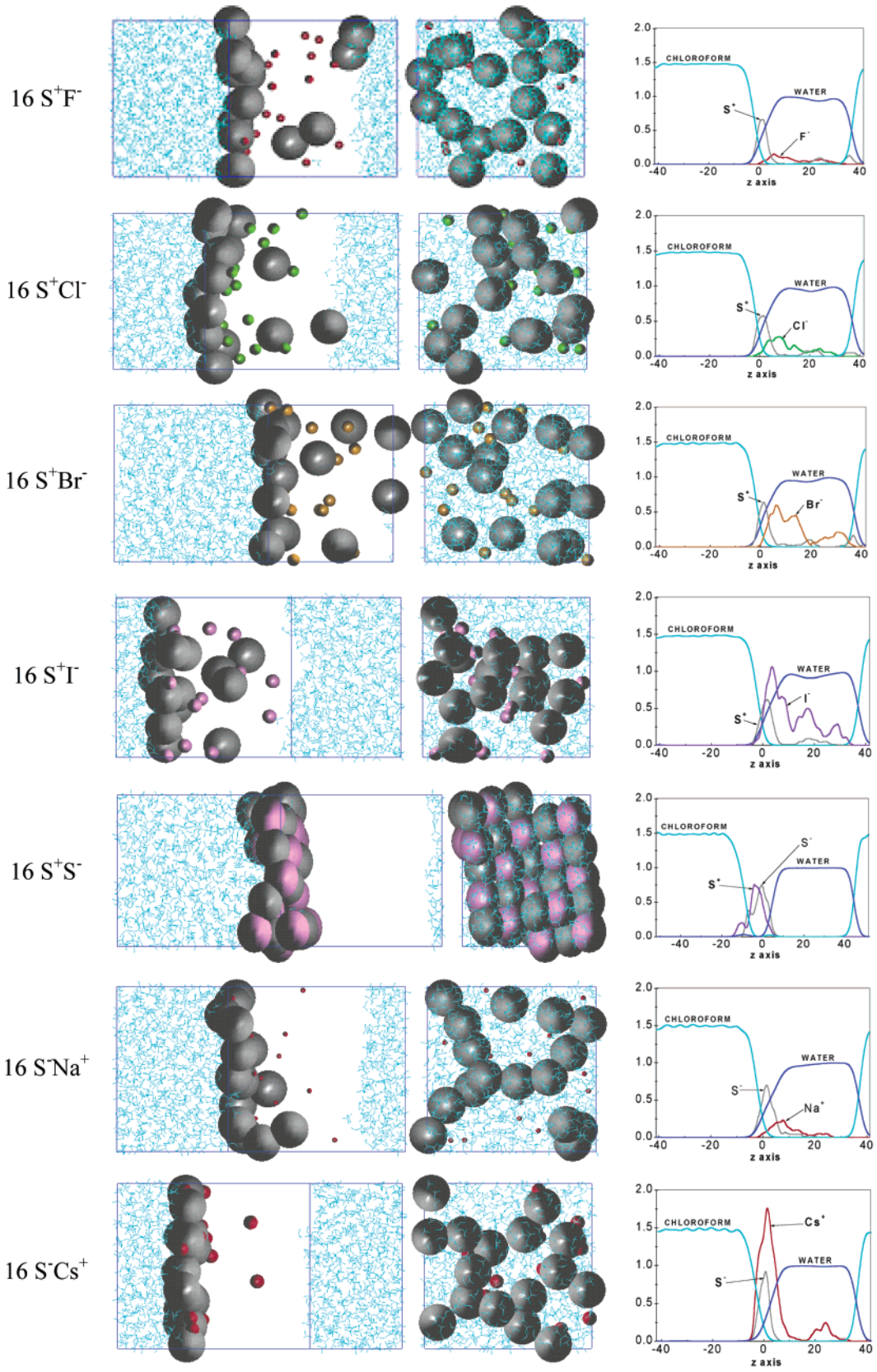


**Figure 3.** Solutions of 16 $S^+$ $X^-$ (X = F / Cl / Br / I / S) and 16 $S^-$ $M^+$ (M = Na / Cs) ions at the interface. Final snapshot after 1.5 ns of dynamics (views from the *y* axis and from the *z* axis with water omitted for clarity) and density curves (averages over the last 0.3 ns). PME calculations.

attraction of $S^+$ by $Na^-$ counterions into the aqueous phase, and $S^+\cdots S^+$ repulsion at the interface. Ion sign reversal is also found to change the extent of self-aggregation between like-hydrophobic spheres: according to the average S···S RDFs (Figure S1), these display short contacts, and integration (up to 12 Å) leads to 2.04 $S^-$ per $S^-$, and only 0.65 $S^+$ per $S^+$, thus supporting more self-aggregation for the $S^-$ than for the $S^+$ species.

Comparison of the interfacial potentials shows that there is no simple +/− inversion (Figure 7), because of the differences

**TABLE 4: Solutions of 16 $S^+X^-$ and 16 $S^-M^+$ Ions at the Interface: Main Characteristics of the Density Curves and Average Interaction Energies ($E$ in kcal/mol)[d] and PME Simulations**

| | 16 $S^+X^-$ | | | | | 16 $S^-M^+$ | | |
|---|---|---|---|---|---|---|---|---|
| | $F^-$ | $Cl^-$ | $Br^-$ | $I^-$ | $S^-$ | $Na^+$ | $Cs^+$ | $S^+$ |
| $d$(S···interface)[a] | 1.6 | 1.7 | 1.4 | 1.5 | 0 | 1.3 | 0.6 | 0 |
| $d$(counterions···interface)[a] | *b* | 5.6 | 5.4 | 3.5 | 0 | *b* | 1.8 | 0 |
| % of $S^{\pm}$ at interface[c] | 87 ± 2 | 84 ± 3 | 84 ± 4 | 80 ± 2 | 100 ± 0 | 93 ± 2 | 100 ± 0 | 100 ± 0 |
| % of $X^-$ or $M^+$ at interface[c] | 38 ± 8 | 42 ± 9 | 46 ± 9 | 52 ± 6 | 100 ± 0 | 50 ± 8 | 80 ± 5 | 100 ± 0 |
| $E_{S^+/X^-}$ or $E_{S^-/M^+}$ | −14 ± 2 | −19 ± 1 | −19 ± 3 | −31 ± 4 | −65 ± 1 | −26 ± 3 | −62 ± 7 | −65 ± 1 |
| $E_{S/wat}$ | −35 ± 2 | −33 ± 2 | −30 ± 3 | −24 ± 3 | −1 ± 1 | −52 ± 3 | −15 ± 3 | −9 ± 4 |

[a] Distance (in Å) between the average ion density peak and the starting interface. [b] Value not reported because the peak is ill-defined. [c] Within 8 Å from the interface. [d] Calculated with RF and a 15 Å cutoff during the last 0.3 ns for 16 $S^+X^-$ and the last 0.2 ns for 16 $S^-M^+$ systems.

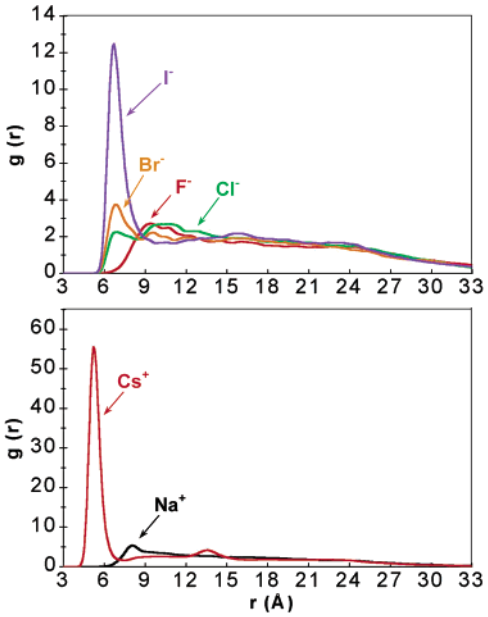


**Figure 4.** Solutions of 16 $S^+$ $X^-$ (X = F/Cl/Br/I/S) and 16 $S^-$ $M^+$ (M = Na/Cs) ions at the interface. Average RDFs between $S^+$ and $X^-$ (top) and between $S^-$ and $M^+$ (bottom). PME calculations.

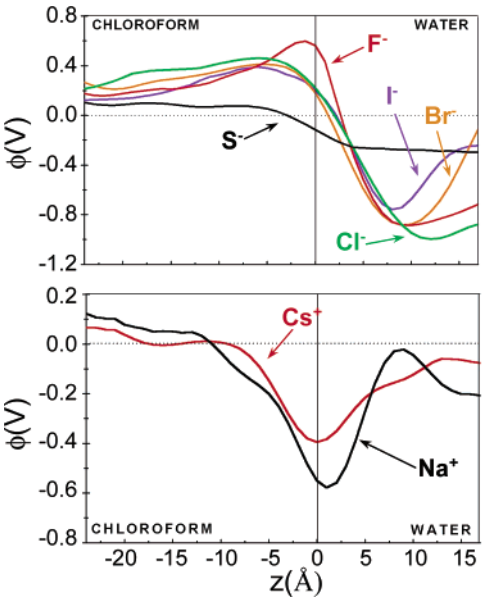


**Figure 5.** Top: Solutions of 16 $S^+$ $X^-$ (X = F (red)/Cl (green)/Br (orange)/I (blue)/S (black)). Bottom: Solutions of 16 $S^-$ $M^+$ (M = Na (black)/Cs (red)) ions at the interface. Average electrostatic potentials $\phi$ (in volts) as a function of $z$. PME calculations.

in ion distributions and solvation. As the interface is more neutralized with $S^-$ $Na^+$ than with $S^+$ $Na^-$ solutes, the $\Delta\phi$ difference between the $\phi_{Max}$ and $\phi_{Min}$ potentials is smaller for the $S^-$ $Na^+$ (0.56 V) than for the $S^+$ $Na^-$ solution (1.32 V).

When the ion charge is increased from ±1 to ±2, its affinity for water should increase by a factor of 4, according to the Born model[65] at constant ionic radius. The ions thus become more hydrophilic and are expected to migrate from the interface to water. This is indeed the observed trend (Figure 6) but, again, the final distribution depends on the sign of the charge. Both $S^{2-}$, $2Na^+$ and $S^{2+}$, $2Na^-$ systems display an equilibrium between S ions at the interface and in water, by different amounts, though. One finds 32% of $S^{2-}$ and 15 ± 4% of $S^{2+}$ species near the interface, corresponding to 30% of $Na^+$ and to 27 ± 6% of $Na^-$ counterions, respectively. Thus, it looks as if $S^{2-}$ ions are more surface active than $S^{2+}$, following the same trend as their monocharged analogues. In both $S^{2-}$- and $S^{2+}$-containing systems one observes another interesting feature, i.e., the self-aggregation of like-charged S ions, which dynamically exchange between dimers and trimers, despite their mutual electrostatic repulsion and high affinity for water. According to the RDFs, there are close S···S contacts, and integration up to 12 Å [66] leads to 0.14 ($S^{2+}$···$S^{2+}$) and 0.06 ($S^{2-}$···$S^{2-}$) ions, respectively, in contact on the average per S species. The S··· Na RDFs (Figure S1) display a marked peak at ≈9 Å, which corresponds to solvent- separated ion pairs of $Na^+$···$OH_2$···$S^{2-}$ or $Na^-$···$H_2O$···$S^{2+}$ types (see Figure 8). In contrast to what was observed with monovalent ions, there are thus no intimate ion pairs, due to the higher affinity of the divalent $S^{2\pm}$ ions for water. Thus, to summarize, inversion of the sign of the electrolyte species yields important differences in their distribution at the interface. A similar conclusion has been obtained for charge surfactant (sodium dodecyl sulfate) monolayers at the water−$CCl_4$ interface.[58]

## Discussion and Conclusion

Molecular dynamics simulations on ion distribution at the interface between two immiscible liquids reveal contrasted behaviors, depending on the size and charge of the ions and counterions. In this section, we first address a number of methodological questions, with the main aim to determine to what extent the simulated distribution of ions are method dependent. This is followed by implications for the mechanism of ion complexation and transfer.

**Methodological Issues.** A first question concerns the sampling of the system, and we note that all starting distributions were "reversed", i.e., with the hydrophilic ions in the organic phase, and all rearranged to expected distributions. For the $S^+$ $S^-$ concentrated solution, two different initial arrangements were found to converge to the same final distribution. We also performed a mixing−demixing simulation of the 16 $S^+$ $Cl^-$ system, in the same conditions as above. Typical snapshots can

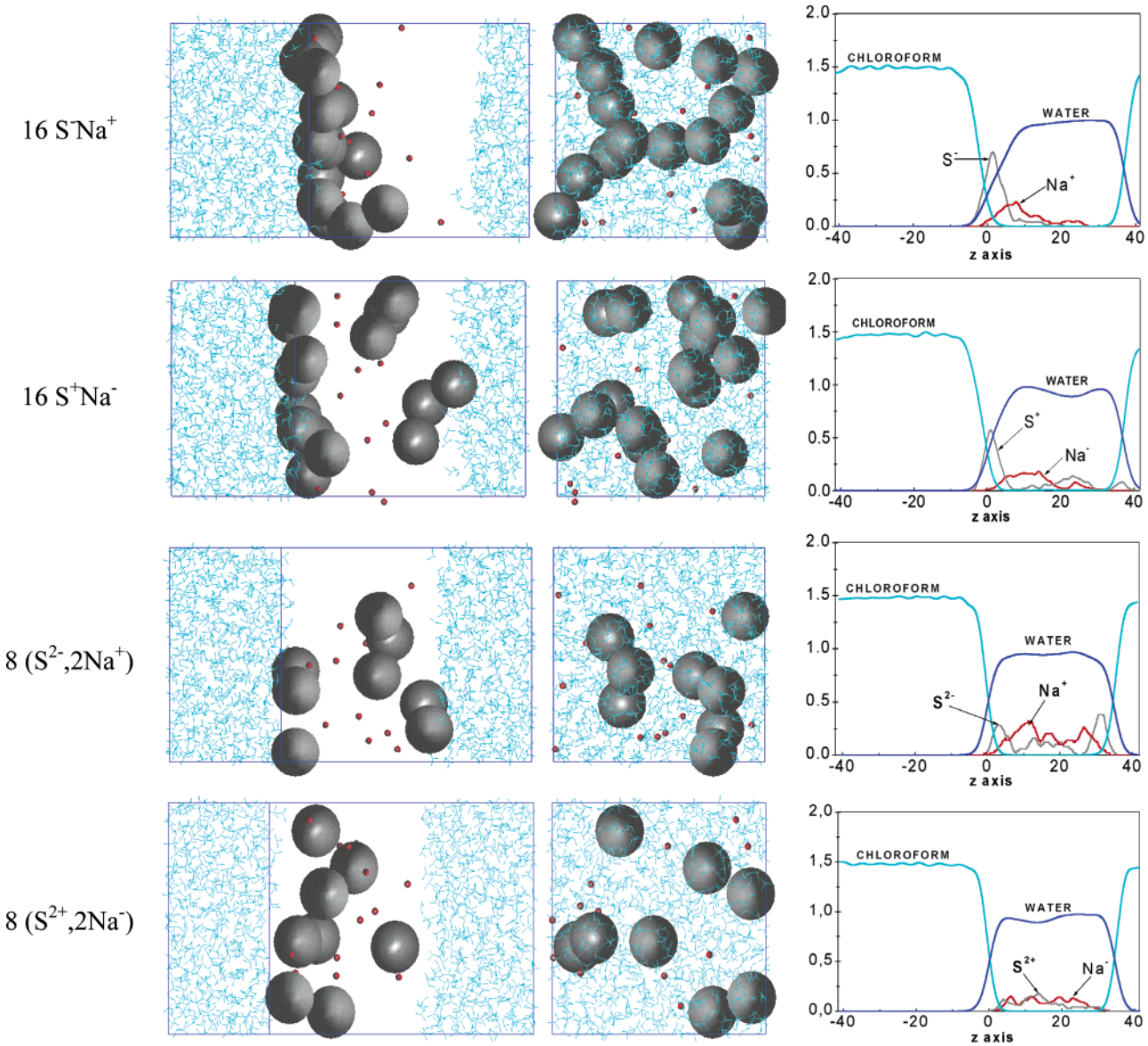


**Figure 6.** Solutions of 16 $S^-$ $Na^+$, 16 $S^+$ $Na^-$, 8 ($S^{2+}$, $2Na^-$), and 8 ($S^{2-}$, $2Na^+$) ions. Final snapshot after 1 ns of dynamics (views from the *y* axis and from the *z* axis with water omitted for clarity) and density curves (averages over the last 0.2 ns). PME calculations.

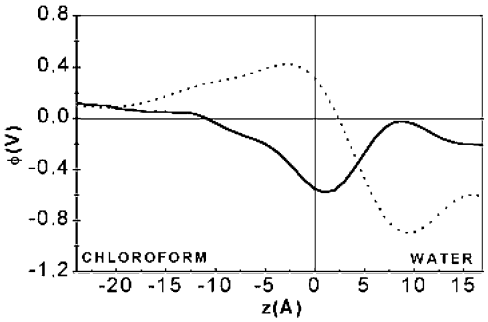


**Figure 7.** Tp: Solutions of 16 $S^-$ $Na^+$ (full line) 16 $S^+$ $Na^-$ (dotted line). Average electrostatic potentials $\phi$ (in volts) as a function of *z*. PME calculations.

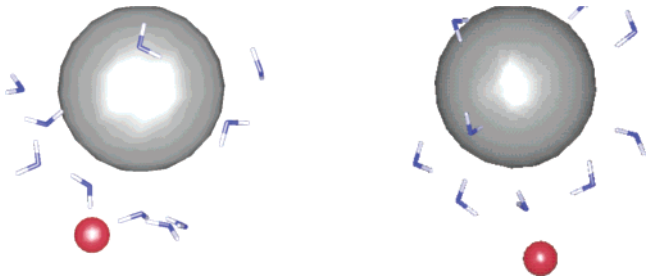

**Figure 8.** Solutions of 8 ($S^{2+}$, $2Na^-$) (left) and 8 ($S^{2-}$, $2Na^+$) (right) ions. Snapshots of typical solvent (water) separated ion pairs.

be seen in Figure 9. Initially, the two liquid phases were completely mixed and the ions "randomly distributed" but, after 0.5 ns, they formed two solvent slabs linked by two interfaces, onto which all $S^+$ ions adsorb and tend to aggregate in dimers or trimers, while all $Cl^-$ anions plus two $S^+$ cations sit in water. The major difference with the simulation at the preformed interface is that the $S^+$ ions diluted onto the two interfaces, instead of concentrating on a single one. Higher ion concentrations would thus be needed to saturate one of them.

Another issue concerns the choice of (*N*,*V*,*T*) thermodynamic ensemble for the simulations. Alternatives, such as (*N*,*P*,*T*) or (*N*,$\gamma$,*T*) ensembles, might be considered as well, possibly modifying the interfacial pressure and detailed distribution of the adsorbed species.[67−70] We thus decided to simulate the 16 $S^+$ $I^-$ and 16 $S^+$ $F^-$ systems for 1.5 ns at a constant pressure of 1 atm, in the same conditions as for the reported (*N*,*V*,*T*) simulations. Again, the majority of $S^+$ ions (77% and 91%,

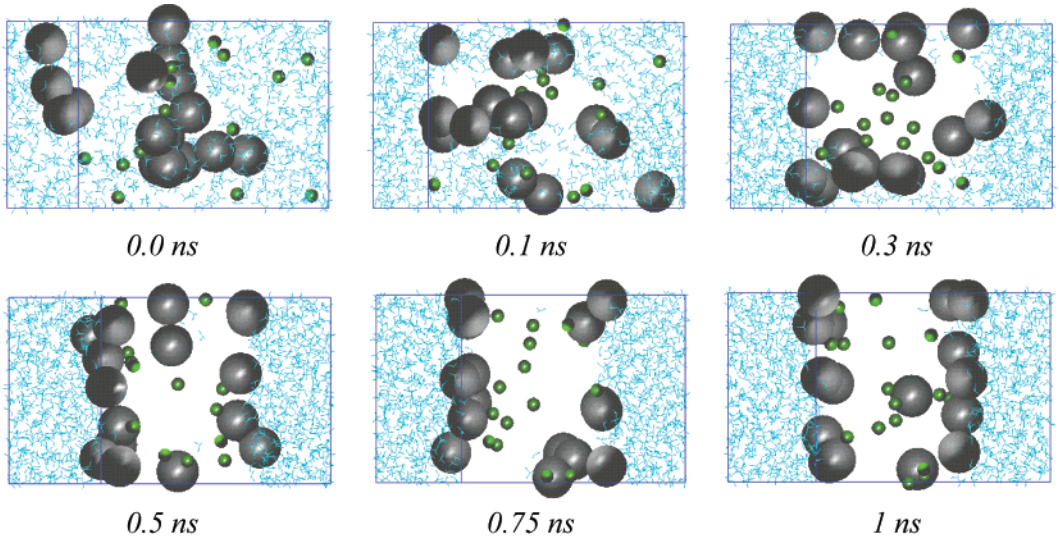


**Figure 9.** Demixing of the water−chloroform binary solution of 16 $S^+$ $Cl^-$. Snapshots at 0, 0.1, 0.3, 0.5, 0.75, and 1.0 ns. Water omitted for clarity. PME calculations.

**TABLE 5: Solutions of 16 $S^+$ $X^-$ (X = F/I) Ions at the Interface. Methodological Tests: (N,P,T) Simulations and (N,V,T) Simulations with Polarization on Water Only ($POL_{wat}$) or on Water + Anions ($POL_{wat+X}$); PME Calculations**

| | 16 $S^+F^-$ | | | 16 $S^+I^-$ | | |
|---|---|---|---|---|---|---|
| | (N,P,T) | $POL_{wat}$ | $POL_{wat+X}$ | (N,P,T) | $POL_{wat}$ | $POL_{wat+X}$ |
| $d$(S···interface)[a] | 1.0 | 1.7 | 1.5 | 0.7 | 0.2 | −0.1 |
| $d$(counterions···interface)[a] | *b* | 4.9 | 6.6 | 3.2 | 1.4 | 2.0 |
| % of $S^{\pm}$ at interface[b] | 91 ± 2 | 97 ± 3 | 91 ± 1 | 77 ± 4 | 98 ± 2 | 100 ± 0 |
| % of $X^-$ or $M^+$ at interface[b] | 35 ± 8 | 89 ± 2 | 85 ± 7 | 62 ± 5 | 92 ± 6 | 94 ± 6 |
| $E_{S^+/X^-}$ | −14 ± 2 | −34 ± 2 | −28 ± 2 | −35 ± 2 | −53 ± 4 | −59 ± 4 |
| $E_{S/wat}$ | −38 ± 2 | −21 ± 2 | −23 ± 2 | −19 ± 2 | −10 ± 2 | −7 ± 2 |

[a] Distance (in Å) between the average ion density peak and the starting interface. [b] Within 8 Å from the interface.

respectively) form an interfacial layer, while some diffused in water or to the other interface (see Figure S2). The anion concentration at the interface is again higher with $I^-$ (62%) than with $F^-$ (35%), and these concentrations are similar to those obtained with the (*N*,*V*,*T*) simulations.

A similar interfacial landscape is observed when simulations are performed for 1 ns on the 16 $S^+I^-$ and 16 $S^+F^-$ systems with the polarizable water model only ($POL_{wat}$), as well as with polarization on water and anions ($POL_{wat+X}$). See Figure S2 and Table 5. The $F^-$- vs $I^-$-containing systems display similar trends as with standard 1-6-12 potentials, but the interfacial concentrations of $S^+$ and $X^-$ ions are somewhat higher. This is consistent with the observation made by others on the increased surface activity of ions when the solvent and anion polarization are incorporated in the force field.[71−75] As a result of polarization, the proportion of $S^+I^-$ cation−anion pairing increases: integration of the $S^+\cdots X^-$ RDFs leads to 0.96 (no polarization), 1.49 ($POL_{wat}$), and 1.87 ($POL_{wat+X}$) anions in contact with a given $S^+$, on the average (Figure S3). For the $S^+F^-$ solution, there is much less ion pairing and the trend is less regular, due to the larger hydration of $F^-$, compared to $I^-$: one finds 0.22 (no polarization), 0.49 ($POL_{wat}$), and 0.24 ($POL_{wat+X}$) $F^-$ per $S^+$. The three models confirm the dominant proportion of intimate ion pairs with $I^-$, compared to $F^-$, related to the weaker affinity of $I^-$ for water. Enhanced ion pairing corresponds to enhanced cation−anion interaction energies and to decreased $S^+$ ion hydration due to reduced accessibility to the solvents (Table 5). The average number of water protons hydrogen bonded to the anion is 7 (without polarization), 6 ($POL_{wat}$), and 6 ($POL_{wat+X}$) for $F^-$ (RDF integration up to 2.7 Å) and respectively 7, 5.5, and 5 for $I^-$ (up to 3.5 Å), thus confirming the reduced contacts of $I^-$ with water, compared to $F^-$, and the decreased hydration numbers of a given anion $X^-$ when polarization is added.

Another important issue concerns the treatment of electrostatics and the comparison of the Ewald vs RF results, performed in the 16 $S^+X^-$ series. The final RF distributions and density curves are given in Figure S4 and their characteristics are summarized in Table 6. They follow the same trends as the PME results, but the amount of $S^+$ ions at the interface is larger: they all (100%) adsorbed at the starting interface or migrated to the second one, thus none being immersed in the bulk water. It thus looks as if $S^+$ ions are more hydrophobic and surface active with RF than with PME calculations. The main reasons can be found (i) in the lessened $S^+\cdots S^+$ repulsion at the interface, and (ii) lessened $S^+\cdots X^-$ attractions, which are both quasi-zeroed beyond the cutoff distance of 15 Å with the RF method. Thus, the neglect of long-range electrostatic interactions somewhat exaggerates the interfacial activity of the hydrophobic cations, but leads to similar trends in counterion distributions at the interface (see Table 6): $F^-$ (28%) < $Cl^-$ (35%) < $Br^-$ 38%) < $I^-$ (53 ± 7%) ≪ $S^-$ (100%). The proportion of anions at the interface (and hence, the average cation/anion interaction energies) is, however, smaller with RF than with PME simulations (see Tables 4 and 6). The electrostatic profiles $\phi(z)$ (Figure S5) are similar with the two methods, with positive values at the interface and in the organic phase, and negative values on the water side, but $\Delta\phi$ differences are larger with the RF method, as expected. In contrast to the PME results, there is no regular trend in these $\Delta\phi$ values (in volts): 4.6 for $F^-$ and $I^-$, 5.6 for $Cl^-$, 5.0 for $Br^-$, and 2.7 for $S^-$.

When compared to the ion distribution previously obtained without corrections for the electrostatics (i.e. with standard residue based cutoffs; see refs 33 and 34), both PME and RF

**TABLE 6: Solutions of 16 $S^+X^-$ (X = F / Cl / Br / I / S) Ions at the Interface: Main Characteristics of the Average Density Curves and Average Interaction Energies (in kcal·mol$^{-1}$);[d] RF Simulations**

| | $F^-$ | $Cl^-$ | $Br^-$ | $I^-$ | $S^-$ |
|---|---|---|---|---|---|
| $d(S^+\cdots\text{interface})$[a] | −0.2 | −0.2 | −0.3 | −0.3 | 0 |
| $d(X^-\cdots\text{interface})$[a] | *b* | 9.0 | 8.9 | 3.9 | 0 |
| % of $S^+$ at interface[c] | 100 ± 0 | 100 ± 0 | 100 ± 0 | 100 ± 2 | 100 ± 0 |
| % of $X^-$ at interface[c] | 28 ± 9 | 35 ± 9 | 38 ± 9 | 53 ± 7 | 100 ± 0 |
| $E_{S^+/X^-}$ | −8 ± 2 | −9 ± 2 | −10 ± 2 | −26 ± 3 | −66 ± 1 |
| $E_{S+/wat}$ | −32 ± 3 | −32 ± 2 | −30 ± 3 | −20 ± 2 | 2 ± 1[d] |

[a] Distance (in Å) between the average ion density peak and the starting interface. [b] Value not reported because the peak is ill-defined. [c] Within 8 Å from the interface. [d] $E_{S^-/wat} = -18 \pm 1$ kcal.mol$^{-1}$.

results markedly differ as far as the $S^+/X^-$ relationship is concerned. Uncorrected treatments yield zeroed interfacial concentration of anions. The latter were fully immersed in water and separated from the cationic $S^+$ layer, without forming intimate or solvent-separated ion pairs, and thus leading to exaggerated interfacial potentials. As a result, repulsion between hydrophobic ions is not compensated by counterions at the interface, which may artifactually engender the expulsion of some of them to the organic phase.[34]

**Interfacial Ion Distribution and the Mechanism of Assisted Ion Transfer.** The methodological tests presented above confirm the surface activity of large spherical ions with pronounced counterion effects. The studied S ions can be viewed as simple models of ion complexes formed with hydrophobic extractant molecules (e.g. cryptates, calixarenes), and the results have implications as far as the mechanism of assisted ion transfer through hydrophobic membranes is concerned. They make clear that the complexes, although hydrophobic, accumulate at the water−"oil" interface instead of migrating to the organic phase, and that this is strongly dependent on counterions.

A first issue concerns the cation complexation process, i.e., under which circumstances hydrophobic ligands meet hydrophilic cations. Hydrophobic anions (fatty acid derivatives, dicarbollides, phenolate derivatives) facilitate the cation extraction because of their favorable partition coefficient. For instance, the free energy of transfer from water to nitrobenzene increases in the following series: cobalt−dicarbollyl < dipicrylaminate < $I_5^-$ < $BPh_4^-$ < $I_3^-$ < Picrate < $ClO_4^-$ < $I^-$ < $Br^-$ < $Cl^-$.[2,76] What happens at the interface is also crucial.[5] Like $S^-$ species, hydrophobic (and, a fortiori amphiphilic) anions accumulate at the interface and the resulting negative potential attracts cations (e.g. $Na^+$, $Cs^+$) which would otherwise be "repelled" by the interface,[77] thus facilitating their capture by interfacial ligands. The ion uptake and recognition thus takes place at the interface, leading to the formation of a hydrophobic complex. We note that complexes should be still more surface active than the simulated S species are, due to specific hydration patterns and generally asymmetrical structures. See for instance refs 29, 55, 56, and 78. As suggested by experiments on anion transport through hydrophobic membranes or on anion capture at a NaCl aqueous interface, even tetracharged macrocyclic hosts of tetrahedral shape are surface active,[79,80] and this is consistent with simulation results.[81] The calculated counterion effect is also consistent with electrochemical studies on the interface between aqueous solutions of alkali halides and a solution of $AsPh_4^+$ $BPh_4^-$ in 1,2-dichlorethane, where the increase in capacity of the interface from $Li^+$ to $Cs^+$ was attributed to ion pairing.[82] A similar picture emerges from surface tension measurements on ammonium salts with different counterions.[83] Our results are also consistent with recent simulations on the Hofmeister effect, according to which large anions penetrate more deeply into a phosphatidinecholine bilayer than do the $Cl^-$ anions.[84] The effect of counterions on molecular transport across a bilayer,[85] as well as the accumulation of $AsPh_4^+$ $BPh_4^-$ species (analogous of $S^+$ $S^-$) at an aqueous interface with 1,2-dichloroethane,[86] has been recently probed by spectroscopy.

Thus, even quasispherical charged complexes are surface active, which rises the question of their migration from the interface to the organic phase. Adding neutralizing hydrophobic species may not be sufficient for that purpose, as shown by the simulation on $S^+$ $S^-$ salt that forms a neutral layer ("crust") at the interface, instead of migrating to the oil phase. We note that our simulated systems are not concentrated enough to locally saturate the interface, and the effect of increased concentration has to be further investigated, possibly leading to modification at interface tension and properties. A recent study on the effect of added neutral synergistic ligands (e.g. tri-*n*-butyl phosphate)[87] shows that the system may evolve from a well-defined interface to a local "third phase" region, and to micelles and microemulsions. What happens with charged species remains to be investigated. This is not without analogy with the effect of counterions (e.g. $Cl^-$ vs $Br^-$ vs $I^-$) on the aggregation and micellar structure of surfactants.[85,88,89]

**Acknowledgment.** The authors are grateful to CNRS-IDRIS and to Université Louis Pasteur for allocation of computer resources, and to Alain Chaumont for his help.

**Supporting Information Available:** RDF plots for S···Na, S···S, S···$H_{wat}$, and S···$O_{wat}$ (Figure S1), plot of (*N*,*P*,*T*) simulations (Figure S2), RDF plots for $S^+\cdots F^-$ and $S^+$ $I^-$ (Figure S3), final RF distributions and density curves (Figure S4), and electrostatic profiles $\phi(z)$ (Figure S5); table of main characteristics of the average density curves and interaction energies for solutions of 16 $S^-$ $Na^+$, 16 $S^+$ $Na^-$, and 8 ($S^{2-}$, $2Na^+$) ions at the interface. This material is available free of charge via the Internet at http://pubs.acs.org.

## References and Notes

(1) Volkov, A. G.; Deamer, D. W.; Tanelian, D. L.; Markin, V. S. *Liquid Interfaces in Chemistry and Biology*; John Wiley & Sons: New York, 1998.

(2) Girault, H. H.; Schiffrin, D. J. In *Electroanalytical Chemistry*; Bard, A. J., Ed.; Dekker: New York, 1989; pp 1−141 and references therein.

(3) Kazarinov, V. E. *The Interface Structure and Electrochemical Processes at the Boundary Between two Immiscible Liquids*; Kazarinov, V. E., Ed.; Springer-Verlag: Berlin, Germany, 1987.

(4) Osipow, L. I. *Surface Chemistry. Theory and Industrial Applications*; Reinhold Publishing Corporation: London, UK, 1962.

(5) Watarai, H. *Trends Anal. Chem.* **1993**, *12*, 313−318.

(6) Schmickler, W. *Interfacial electrochemistry*; Oxford University Press: New York, 1996.

(7) Adamson, A. W. *Physical Chemistry of Surfaces*, 5th ed.; Wiley: New York, 1990.

(8) Koryta, J. *Ion Sel. Electrode Rev.* **1983**, *5*, 131−164.

(9) Eisenthal, K. B. *Chem. Rev.* **1996**, *96*, 1343−1360.
(10) Brevet, P. F. *Surface Second Harmonic Generation*; Cahiers de Chimie, Presses Polytechniques et Universitaires Romandes, 1997.
(11) Rice, S. A. *Nature* **1985**, *316*, 108.
(12) Pershan, P. S. *Faraday Discuss. Chem. Soc.* **1990**, *89*, 231−245.
(13) Torrie, G. M.; Valleau, J. P. *J. Electroanal. Chem.* **1986**, *106*, 69−79.
(14) Matsui, T.; Jorgensen, W. L. *J. Am. Chem. Soc.* **1992**, *114*, 3220.
(15) Heinzinger, K. *Pure Appl. Chem.* **1985**, *57*, 1031−1042.
(16) Spohr, E.; Heinzinger, K. *Electrochim. Acta* **1988**, *33*, 1211−1222.
(17) Benjamin, I. *Science* **1993**, *261*, 1558−1560.
(18) Benjamin, I. *Acc. Chem. Res.* **1995**, *28*, 233−239 and references therein.
(19) Benjamin, I. *Annu. Rev. Phys. Chem.* **1997**, *48*, 407−451 and references therein.
(20) Bopp, P. A.; Kohlmeyer, A.; Spohr, E. *Electrochim. Acta* **1998**, *43*, 2911−2918.
(21) Bandyopadhyay, S.; Shelley, J. C.; Tarek, M.; Moore, P. B.; Klein, M. L. *J. Phys. Chem. B* **1998**, *102*, 6318−6322.
(22) van Buuren, A. R.; Marrink, S.-J.; Berendsen, J. C. *Colloids Surf.* **1995**, *102*, 143−157.
(23) Wipff, G.; Lauterbach, M. *Supramol. Chem.* **1995**, *6*, 187−207.
(24) Wipff, G.; Engler, E.; Guilbaud, P.; Lauterbach, M.; Troxler, L.; Varnek, A. *New J. Chem.* **1996**, *20*, 403−417.
(25) Varnek, A.; Troxler, L.; Wipff, G. *Chem. Eur. J.* **1997**, *3*, 552−560.
(26) Beudaert, P.; Lamare, V.; Dozol, J.-F.; Troxler, L.; Wipff, G. *Solv. Extract. Ion Exch.* **1998**, *16*, 597−618.
(27) Troxler, L.; Wipff, G. *Anal. Sci.* **1998**, *14*, 43−56.
(28) Berny, F.; Muzet, N.; Schurhammer, R.; Troxler, L.; Wipff, G. In *Current Challenges in Supramolecular Assemblies, NATO ARW Athens*; Tsoucaris, G., Ed.; Kluwer Academic Pub.: Dordrecht, The Netherlands, 1998; pp 221−248.
(29) Berny, F.; Muzet, N.; Troxler, L.; Wipff, G. In *Supramolecular Science: where it is and where it is going*; Ungaro, R., Dalcanale, E., Eds.; Kluwer Academic Pub.: Dordrecht, The Netherlands, 1999; pp 95−125 and references therein.
(30) Stoyanov, E.; Smirnov, I.; Varnek, A.; Wipff, G. In *Euradwaste 1999*: *Radioactive Waste Management Strategies and Issues*; Davies, C., Ed.; European Commission: Brussels, 2000; pp 519−522.
(31) Coupez, B.; Wipff, G. *C. R. Chim. Acad. Sci. Paris* **2004**, in press.
(32) Marcus, Y. *Ion Solvation*; Wiley: Chichester, UK, 1985.
(33) Schurhammer, R.; Wipff, G. *New J. Chem.* **1999**, *23*, 381−391.
(34) Berny, F.; Schurhammer, R.; Wipff, G. *Inorg. Chim. Acta* **2000**, *300*−*302* (Special Issue), 384−394.
(35) Schurhammer, R.; Engler, E.; Wipff, G. *J. Phys. Chem. B* **2001**, *105*, 10700−10708.
(36) Schurhammer, R.; Wipff, G. *J. Phys. Chem. A* **2000**, *104*, 11159−11168. Schurhammer, R.; Wipff, G. *J. Phys. Chem. A* **2000**, *105*, 292.
(37) Gouy, G. *J. Phys.* **1910**, *9*, 457.
(38) Chapman, D. L. *Philos. Mag.* **1913**, *25*, 475.
(39) Cacace, M. G.; Landau, E. M.; Ramsden, J. J. *Q. Rev. Biophys.* **1997**, *30*, 241−277.
(40) Case, D. A.; Pearlman, D. A.; Caldwell, J. C.; Cheatham, T. E., III; Ross, W. S.; Simmerling, C. L.; Darden, T. A.; Merz, K. M.; Stanton, R. V.; Cheng, A. L.; Vincent, J. J.; Crowley, M.; Ferguson, D. M.; Radmer, R. J.; Seibel, G. L.; Singh, U. C.; Weiner, P. K.; Kollman, P. A. *AMBER5*, University of California, San Francisco 1997.
(41) Åqvist, J. *J. Phys. Chem.* **1990**, *94*, 8021−8024.
(42) Berny, F. Ph.D Thesis, 2000, Université Louis Pasteur, Strasbourg.
(43) Jorgensen, W. L.; Chandrasekhar, J.; Madura, J. D.; Impey, R. W.; Klein, M. L. *J. Chem. Phys.* **1983**, *79*, 926−936.
(44) Jorgensen, W. L.; Briggs, J. M.; Contreras, M. L. *J. Phys. Chem.* **1990**, *94*, 1683−1686.
(45) Chang, T. M.; Dang, L. X. *J. Chem. Phys.* **1995**, *104*, 6772.
(46) Applequist, J.; Carl, J. R.; Fung, K.-K. *J. Am. Chem. Soc.* **1972**, *94*, 2952−2960.
(47) Daura, X.; Hünenberger, P. H.; Mark, A. E.; Querol, E.; Avilés, F. X.; van Gunsteren, W. F. *J. Am. Chem. Soc.* **1996**, *118*, 6285−6294.
(48) Hummer, G.; Pratt, L. R.; Garcia, A. E. *J. Phys. Chem.* **1996**, *100*, 1206−1215.
(49) Ewald, P. P. *Ann. Phys.* **1921**, *64*, 253.
(50) Darden, T. A.; York, D. M.; Pedersen, L. G. *J. Chem. Phys.* **1993**, *98*, 10089.
(51) Tironi, I. G.; Sperb, R.; Smith, P. E.; van Gunsteren, W. F. *J. Chem. Phys.* **1995**, *102*, 5451−5459.
(52) Spohr, E. *J. Chem. Phys.* **1997**, *107*, 6342−6348.
(53) Dominguez, H.; Smodyrev, A. M.; Berkowitz, M. L. *J. Phys. Chem. B* **1999**, *103*, 9582−9588.
(54) Hautman, J.; Klein, M. L. *Mol. Phys.* **1992**, *75*, 379−395.
(55) Lauterbach, M.; Engler, E.; Muzet, N.; Troxler, L.; Wipff, G. *J. Phys. Chem. B* **1998**, *102*, 225−256.
(56) Muzet, N.; Engler, E.; Wipff, G. *J. Phys. Chem. B* **1998**, *102*, 10772−10788.
(57) Berendsen, H. J. C.; Postma, J. P. M.; van Gunsteren, W. F.; DiNola, A. *J. Chem. Phys.* **1984**, *81*, 3684−3690.
(58) Pratt, L. R. *J. Phys. Chem.* **1992**, *96*, 25−33.
(59) Pierotti, R. A. *Chem. Rev.* **1976**, *76*, 717−726.
(60) Blokzijl, W.; Engberts, J. B. F. N. *Angew. Chem., Int. Ed. Engl.* **1993**, *32*, 2, 1545−1579 and references cited therein.
(61) Schurhammer, R.; Wipff, G. *J. Mol. Struct. THEOCHEM* **2000**, *500*, 139−155. Schurhammer, R.; Wipff, G. *J. Mol. Struct. THEOCHEM* **2001**, *536*, 289.
(62) We note that these $S^+\cdots X^-$ contacts are 1.2 Å longer at the interface and thus looser than in the simulated gas-phase dimers, due to hydration of the ions at the interface.
(63) It should be noted that the origin ($z = 0$), defined as the intersection of the solvent density curves, may be sometimes ill-defined when the interface is quasicovered by the $S^+$ ions, thus leading to weak overlap of the solvent densities.
(64) Not only the ions, but also the solvent contributes to $\Delta\phi$ (by 0.15 V, in the case of the $S^+ S^-$ salt), due to specific orientations of water molecules around the ions and at the interface.
(65) Born, M. *Z. Phys.* **1920**, *1*, 45.
(66) This is the ending distance of the first S···S peak observed with monovalent $S^{\pm}$ ions; see Figure S1.
(67) Feller, S. E.; Zhang, Y.; Pastor, R. W. *J. Chem. Phys.* **1995**, *105*, 4871.
(68) Zhang, Y.; Feller, S. E.; Brooks, B. R.; Pastor, R. W. *J. Chem. Phys.* **1995**, *103*, 10252.
(69) Tieleman, D. P.; Berendsen, H. J. C. *J. Chem. Phys.* **1996**, *105*, 4871−4880.
(70) Alejandre, J.; Tildesley, D. J.; Chapela, G. A. *J. Chem. Phys.* **1995**, *102*, 4574−4583.
(71) Dang, L. X. *J. Phys. Chem. B* **1999**, *103*, 8195−81200.
(72) Dang, L. X. *J. Phys. Chem. B* **2001**, *105*, 804−809.
(73) Jungwirth, P.; Tobias, D. J. *J. Phys. Chem. A* **2002**, *106*, 379−383.
(74) Yoo, S.; Lei, Y. A.; Zeng, X. C. *J. Chem. Phys.* **2003**, *119*, 6083−6091.
(75) Dang, L. X. *J. Phys. Chem. B* **2002**, *106*, 10388−10394.
(76) Koryta, J.; Vanysek, P.; Brezina, M. *J. Electroanal. Chem.* **1977**, *75*, 211−228.
(77) Fernandes, P. A.; Cordeiro, M. N. D. S.; Gomes, J. A. N. F. *J. Phys. Chem. B* **2001**, *105*, 981−993.
(78) Baaden, M.; Berny, F.; Muzet, N.; Troxler, L.; Wipff, G. In *Calixarenes for Separation*; ACS Symp. Ser. 757; Lumetta, G., Rogers, R., Gopalan, A., Eds.; American Chemical Society: Washington, DC, 2000; pp 71−85.
(79) Ichikawa, K.; Hossain, M. A.; Tamura, T.; Kamo, N. *Supramol. Chem.* **1995**, *5*, 219−224.
(80) Ichikawa, K.; Yamada, M.; Ito, N. *Chem. Eur. J.* **1998**, *4*, 914−918.
(81) Chaumont, A.; Wipff, G. *J. Comput. Chem.* **2002**, *23*, 1532−1543.
(82) Cheng, Y.; Cunnane, V. C.; Schriffin, D. J.; Mutomäki, L.; Kontturi, K. *J. Chem. Soc., Faraday Trans.* **1991**, *87*, 107.
(83) Popov, A. N. In *The Interface Structure and Electrochemical Processes at the Boundary Between two Immiscible Liquids*; Kazarinov, V. E., Ed.; Springer-Verlag: Berlin, Germany, 1987; pp 179−205 and references therein.
(84) Sachs, J. N.; Woolf, T. B. *J. Am. Chem. Soc.* **2003**, *125*, 8742−8743.
(85) Shang, X.; Liu, Y.; Yan, E.; Eisenthal, K. B. *J. Phys. Chem. B* **2001**, *105*, 12816−12822.
(86) Conboy, J. C.; Richmond, G. L. *J. Phys. Chem. B* **1997**, *101*, 983−990.
(87) Coupez, B.; Boehme, C.; Wipff, G. *J. Phys. Chem. B* **2003**, *107*, 9484−9490.
(88) Askal, V. K.; Goyal, P. S. *Chem. Phys. Lett.* **2003**, *368*, 59−65 and references cited therein.
(89) For the cationic dodecyltrimethylammonium and dodecylpyridinium salts, the order of decreasing critical micellar concentration "cmc" in aqueous medium is $F^- > Cl^- > Br^- > I^-$. Similarly, in the case of the anionic surfactant lauryl sulfates, the cmc decreases in the order of counterions $Li^+ > Na^+ > K^+ > Cs^+ > NMe_4^+ > NEt_4^+ > Ca^{2+} > Mg^{2+}$. See: Srinivasan, V.; Blankschtein, D. *Langmuir* **2003**, *19*, 9932−9945. Rosen, M. J. *Surfactants and Interfacial Phenomena*; John Wiley & Son: New York, 1989.